Bansal et al. EJNMMI Research (2015) 5:19
DOI 10.1186/s13550-015-0098-y

EJNMMI Research
a SpringerOpen Journal

ORIGINAL RESEARCH Open Access

# Novel $^{89}$Zr cell labeling approach for PET-based cell trafficking studies

Aditya Bansal[1], Mukesh K Pandey[1], Yunus E Demirhan[1], Jonathan J Nesbitt[2], Ruben J Crespo-Diaz[2], Andre Terzic[2], Atta Behfar[2] and Timothy R DeGrado[1*]

## Abstract

**Background:** With the recent growth of interest in cell-based therapies and radiolabeled cell products, there is a need to develop more robust cell labeling and imaging methods for *in vivo* tracking of living cells. This study describes evaluation of a novel cell labeling approach with the positron emission tomography (PET) isotope $^{89}$Zr ($T_{1/2}$ = 78.4 h). $^{89}$Zr may allow PET imaging measurements for several weeks and take advantage of the high sensitivity of PET imaging.

**Methods:** A novel cell labeling agent, $^{89}$Zr-desferrioxamine-NCS ($^{89}$Zr-DBN), was synthesized. Mouse-derived melanoma cells (mMCs), dendritic cells (mDCs), and human mesenchymal stem cells (hMSCs) were covalently labeled with $^{89}$Zr-DBN via the reaction between the NCS group on $^{89}$Zr-DBN and primary amine groups present on cell surface membrane protein. The stability of the label on the cell was tested by cell efflux studies for 7 days. The effect of labeling on cellular viability was tested by proliferation, trypan blue, and cytotoxicity/apoptosis assays. The stability of label was also studied in *in vivo* mouse models by serial PET scans and *ex vivo* biodistribution following intravenous and intramyocardial injection of $^{89}$Zr-labeled hMSCs. For comparison, imaging experiments were performed after intravenous injections of $^{89}$Zr hydrogen phosphate ($^{89}$Zr(HPO$_4$)$_2$).

**Results:** The labeling agent, $^{89}$Zr-DBN, was prepared in 55% ± 5% decay-corrected radiochemical yield measured by silica gel iTLC. The cell labeling efficiency was 30% to 50% after 30 min labeling depending on cell type. Radioactivity concentrations of labeled cells of up to 0.5 MBq/10$^6$ cells were achieved without a negative effect on cellular viability. Cell efflux studies showed high stability of the radiolabel out to 7 days. Myocardially delivered $^{89}$Zr-labeled hMSCs showed retention in the myocardium, as well as redistribution to the lung, liver, and bone. Intravenously administered $^{89}$Zr-labeled hMSCs also distributed primarily to the lung, liver, and bone, whereas intravenous $^{89}$Zr(HPO$_4$)$_2$ distributed to the liver and bone with no activity in the lung. Thus, the *in vivo* stability of the radiolabel on the hMSCs was evidenced.

**Conclusions:** We have developed a robust, general, and biostable $^{89}$Zr-DBN-based cell labeling strategy with promise for wide applications of PET-based non-invasive *in vivo* cell trafficking.

**Keywords:** Zirconium-89, PET; Cell labeling; *In vivo* cell tracking

* Correspondence: DeGrado.Timothy@mayo.edu
[1]Department of Radiology, Mayo Clinic, Rochester 55905, MN, USA
Full list of author information is available at the end of the article

## Background

With the growth of interest in cell-based therapies, there is a need to develop more sensitive, robust, and quantitative imaging methods for *in vivo* tracking of living cells. A number of radioisotopic cell labeling methods have traditionally been used for single-photon emission computerized tomography (SPECT) and positron emission tomography (PET) imaging-based cell tracking [1]. However, a PET-based approach would offer superior quantification and imaging sensitivity characteristics over a SPECT-based approach, which are critical for tracking of small numbers of administered cells [1]. In this regard, $^{89}$Zr has emerged as an attractive PET radionuclide for cell labeling applications due to its high spatial resolution and 78.4-h half-life that may allow monitoring of administered cells up to a 2- to 3-week period.

A variety of cell labeling strategies have been forwarded, including transport of a radiometal ($^{111}$In, $^{99m}$Tc, $^{64}$Cu, $^{89}$Zr) into cells in conjunction with oxine, hexamethylpropyleneamine oxime (HMPAO), pyruvaldehyde-bis(N4-methylthiosemicarbazone) (PTSM), or protamine sulfate, or antibody-based labeling (Table 1) [1-11]. In the transport approach, after entry into the cell, the radiometal dissociates and binds to a variety of intracellular biomolecules. The major drawback of this approach is that appreciable efflux of sequestered radioactivity is observed post-labeling. The extent of efflux has been as high as 70% to 80% in 24 to 96 h as reported for $^{111}$In-oxine-labeled lymphocytes [4], $^{111}$In-oxine-labeled hematopoietic progenitor cells [5], and $^{64}$Cu-PTSM-labeled C6 glioma cells [7]. Recently, $^{89}$Zr-oxine has been reported as a labeling molecule but like $^{111}$In-oxine, it also undergoes efflux (10% to 29% at 24 h in macrophages, breast cancer cells, and myeloma cells [9] and 70% to 80% at 24 h in natural killer cells [10]). Efflux of radiolabel significantly limits monitoring cell trafficking over longer observational periods. Cells have also been labeled with $^{18}$F-FDG [12-16] ($T_{1/2}$ = 109.8 min), $^{99m}$Tc-HMPAO [17] ($T_{1/2}$ = 6 h), and $^{64}$Cu-labeled anti-CD45 [8] ($T_{1/2}$ = 12.7 h), but the short half-lives of these radioisotopes limit their utility for cell tracking to shorter observational periods. An alternative antibody-based stem cell labeling method employed $^{89}$Zr-labeled anti-CD45 for *ex vivo* labeling of stem cells expressing CD45 membrane protein. However, this radiotracer yielded poor *in vivo* imaging characteristics, possibly due to insufficient CD45 molecules on the plasma membrane of stem cells [8].

In this study, we propose a novel cell labeling strategy that covalently binds a $^{89}$Zr-DFO-labeled agent to cell surface proteins independent of cell type. The novel method employs the two-step process (Figure 1): 1) preparation of $^{89}$Zr-labeled *p*-isothiocyanato-benzyl-desferrioxamine ($^{89}$Zr-DBN) and 2) random labeling of primary amines of cell surface proteins with $^{89}$Zr-DBN. We have evaluated this labeling strategy in three cell types: mouse melanoma cells (mMCs), human mesenchymal stem cells (hMSCs), and mouse dendritic cells (mDCs). The labeled cells were evaluated for 7 days post-labeling for label retention and probable changes in cell proliferation, cell viability, and degree of apoptosis in radiolabeled cells as compared to their

**Table 1 Present direct radioisotopic cell labeling methods**

| Isotope-compound/$T_{1/2}$ | Cells labeled | Labeling and imaging characteristics | Reference |
|---|---|---|---|
| $^{111}$In-oxine/67.4 h | Leukocytes | Approximately 80% cell labeling yield in 30 min | [2-6] |
| | Lymphocytes | Significant efflux rate reported in lymphocytes (approximately 70% effluxed in 24 h) and HPCs (approximately 75% effluxed in 96 h) | |
| | HPCs | Suboptimal image quality and sensitivity | |
| $^{64}$Cu-PTSM/12.7 h | C6 glioma cells | 70% to 85% cell labeling yield in 5 h | [7] |
| | | Significant efflux rate from cells (approximately 80% effluxed in 24 h) | |
| $^{64}$Cu-TETA- or $^{89}$Zr-DFO-antiCD45/12.7 h ($^{64}$Cu), 78.4 h ($^{89}$Zr) | hPBSCs | Binds to only CD45 membrane protein expressing cells | [8] |
| | | Approach was suboptimal possibly due to insufficient CD45 molecules on the plasma membrane of stem cells | |
| $^{89}$Zr-oxine/78.4 h | Myeloma cells and natural killer cells | Approximately 32% cell labeling yield in 30 min | [9,10] |
| | | Significant efflux rate reported for myeloma cells (29% effluxed in 24 h) and natural killer cells (70% to 80% effluxed in 7 days) | |
| | | Loss of cell viability possibly due to oxine exposure | |
| $^{89}$Zr-protamine sulfate/78.4 h | Dendritic cells and T lymphocytes | Approximately 34% cell labeling yield (dendritic cells) in 30 min | [11] |
| | | Approximately 12% cell labeling yield (T lymphocytes) in 30 min | |
| | | Weakly binds to non-specific intracellular biomolecules | |
| | | Efflux rate not reported | |

HPCs, hematopoietic progenitor cells; hPBSCs, human peripheral blood stem cells.

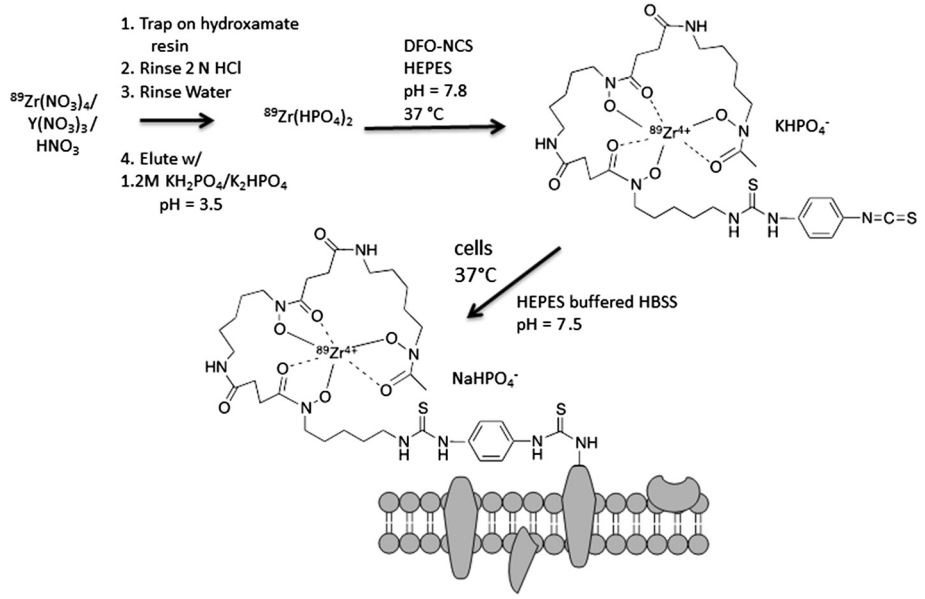


**Figure 1** Scheme for synthesis of $^{89}$Zr-DBN and cell labeling.

unlabeled counterparts. Out of these, labeled hMSCs were further tested for imaging characteristics and stability of radiolabel in an *in vivo* mouse model.

## Methods

### Cell culture

B16-F10 mMCs from ATCC, Manassas, VA, USA, hMSCs from patients, and JAWSII mDCs from ATCC, Manassas, VA, USA, were used for evaluating the $^{89}$Zr-DBN-based labeling method. The mMCs and hMSCs were cultured in complete Dulbecco's modified Eagle's medium (DMEM) (DMEM + 10% FBS), and mDCs were cultured in complete alpha MEM (alpha MEM + 4 mM L-glutamine + 1 mM sodium pyruvate + 5 ng/mL murine GM-CSF + 20% FBS). The cultures were maintained in a humidified cell culture chamber (21% $O_2$, 74% $N_2$, 5% $CO_2$) at 37°C.

### Production and isolation of $^{89}$Zr

$^{89}Zr^{4+}$ was produced in aqueous solution through the $^{89}Y(p,n)^{89}Zr$ nuclear reaction using a solution target containing yttrium nitrate and dilute nitric acid [18]. The $^{89}Zr^{4+}$ was isolated from $^{89}Y^{3+}$ using a hydroxamate resin-based purification method [18,19] with the exception that the final elution of $^{89}Zr^{4+}$ off the hydroxamate resin was performed with an appropriate volume of 1.2 M $K_2HPO_4/KH_2PO_4$ buffer (pH 3.5). The $K_2HPO_4/KH_2PO_4$ buffer was allowed to sit on the column for 30 min before elution to promote release of $^{89}$Zr as zirconium hydrogen phosphate, $^{89}Zr(HPO_4)_2$, from the column. The elution percentage of $^{89}$Zr from the column was approximately 89% collected in four fractions of 0.5 mL each.

### Synthesis of $^{89}$Zr-DBN

The eluted $^{89}Zr(HPO_4)_2$ solution (120 μL) was neutralized to pH 7.8 with 100 μL 1 M HEPES-KOH buffer (pH 7.5) and 65 μL 1 M $K_2CO_3$. To this, 4 μL 5 mM DFO-Bz-NCS in DMSO (Macrocylics, Dallas, TX, USA) was added, and chelation of $^{89}Zr^{4+}$ proceeded at 37°C for 1 h in a thermomixer at 550 rpm. Chelation efficiency was determined by silica gel iTLC (Agilent Technologies, Santa Clara, CA, USA) with 50 mM DTPA pH 7 as the mobile phase. $^{89}$Zr-DBN showed an $R_f = 0$, whereas $^{89}Zr(HPO_4)_2$ had an $R_f = 0.9$.

### Labeling of cells with $^{89}Zr(HPO_4)_2$ and $^{89}$Zr-DBN

The adherent cells were trypsinized and washed once with PBS and twice with HEPES buffered GIBCO Hanks Balanced Salt solution buffered (Thermo Fisher, Waltham, MA, USA) (H-Hank's Balanced Salt Solution (HBSS), pH 7.5. The cell labeling reaction was performed with approximately $6 \times 10^6$ cells in 500 uL H-HBSS at pH 7.5. To this, either 100 μL $^{89}Zr(HPO_4)_2$ (approximately 6 MBq) or 100 uL $^{89}$Zr-DBN (approximately 6 MBq) was added and was allowed to incubate at 37°C for 30 min on a shaker for cell labeling. After incubation, the cells were washed four times with appropriate volume of complete medium. The final labeling efficiency was calculated from the radioactivity bound to cells after all the washes.

### Incorporation of $^{89}$Zr-DBN in protein fraction

To understand the subcellular localization of the label, incorporation of $^{89}$Zr-DBN into different protein fractions in mMCs, hMSCs, and mDCs was evaluated using a subcellular protein fractionation kit (Piercenet Thermo

Scientific, Waltham, MA, USA) at days 1, 4, and 7 post-labeling. The cytosolic proteins, hydrophobic membrane proteins, nuclear proteins, and cytoskeletal proteins were isolated, and each protein fraction was counted for radioactivity using a 2480 Wizard$^2$ automatic gamma counter (PerkinElmer, Waltham, MA, USA).

### Efflux of $^{89}$Zr-DBN from labeled cells

To determine cellular efflux, $0.3 \times 10^6$ $^{89}$Zr-labeled cells were plated into each well of a six-well culture plate. The medium was replaced with fresh medium daily for 7 days, and radioactivity in the replaced medium was counted. For mDCs with mix of adherent and suspension cells, the plate was centrifuged at 1,000 rpm for 10 min before replacing the medium to avoid loss of unattached $^{89}$Zr-labeled cells.

### CyQUANT cellular proliferation assay

The effect of radiolabeling on cellular proliferation was assessed by the CyQUANT DNA content assay (Thermo Fisher, Waltham, MA, USA). A known number of unlabeled and $^{89}$Zr-labeled cells (approximately $10^4$ cells/well) were plated in 21 wells of a 96-well culture plate and maintained at 37°C in a $CO_2$ incubator. The amount of DNA in each well was quantified from absorbance values as a surrogate marker of the number of cells present. The culture medium was replaced daily. The CyQUANT assay was performed for three wells per day over 5 days.

### Trypan blue exclusion assay cellular viability test

The effect of labeling on cellular viability was assessed using trypan blue exclusion assay test within 1 h of labeling, third and seventh day post-labeling. The culture medium was replaced daily and maintained at 37°C in a $CO_2$ incubator. Unlabeled cells served as control.

### ApoTox-Glo viability/cytotoxicity and apoptosis assay

The effect of radiolabeling on cellular viability was also assessed using the ApoTox-Glo viability, cytotoxicity, and caspase 3/7 apoptosis assay (Promega Corporation, Madison, WI, USA). Unlabeled cells served as control. A known number of unlabeled and $^{89}$Zr-labeled cells (approximately $10^4$/well) were plated in a 96-well culture plate. The culture medium was replaced daily and maintained at 37°C in a $CO_2$ incubator. At day 7, cell viability, cytotoxicity, and apoptosis were quantified in triplicate using the ApoTox-Glo assay. As positive controls, cells were incubated with 30 μg/mL digitonin for 30 min for the viability and cytotoxicity assays, while 2 μM staurosporine was added for 16 h for the caspase 3/7 dependent apoptosis assay.

### PET imaging and ex-vivo biodistribution of $^{89}$Zr-labeled cells and $^{89}Zr(HPO_4)_2$

Experiments were performed with 2-month-old athymic nude Foxn1$^{nu}$ mice (Harlan Laboratories, Inc., Indianapolis, IN, USA). $^{89}Zr(HPO_4)_2$ (approximately 0.074 MBq) or $^{89}$Zr-labeled cells ($2 \times 10^5$ cells with radioactivity concentration approximately 0.37 MBq/$1 \times 10^6$ cells) were injected intravenously through a tail vein. On days 2, 4, and 7, the mice were anesthetized under 1% to 2% isoflurane and underwent PET imaging using a small animal PET/X-RAY system (Sofie BioSystems Genesys4, Culver City, CA, USA). At day 7, the mice were sacrificed and tissues were extracted and radioactivity counted using a gamma counter to evaluate the biodistribution of $^{89}$Zr radioactivity. PET images were normalized to units of standardized uptake value (SUV) = (activity concentration in tissue / (injected dose/g whole body wt.)) and presented as a coronal sectional images.

### *In vivo* tracking of stem cell engraftment in ischemia/reperfusion mouse model

Athymic nude Foxn1$^{nu}$ mice (2 months old) were anesthetized under 1% to 2% isoflurane and placed on a heating pad maintained at 37°C. Respiratory and heart rates were monitoring continually. After intubation, mechanical ventilation and intercostal block of bupivacaine and lidocaine, an incision was made in through the fourth or fifth intercostal space for access into the thoracic space, the heart was exposed and the pericardium was incised anterior and parallel to the phrenic nerve. With visualization of the coronary vasculature, the left coronary artery was ligated to induce myocardial ischemia at the anterior wall of the left ventricle. One hour after the coronary ligation, the suture was untied for reperfusion. Myocardial reperfusion was confirmed by color change of the left ventricle and electrocardiographic changes. During reperfusion, $^{89}$Zr-labeled cells ($2 \times 10^5$ cells with radioactivity concentration approximately 0.37 MBq/$10^6$ cells) were injected at four sites within the ischemic region. After myocardial injection, the intercostal space, the chest musculature, and the skin were closed with a 7-0 Ethilon suture. The animals were imaged at day 2, day 5, and day 7 using small animal PET/X-RAY system (Sofie BioSystems Genesys4, Culver City, CA, USA). At day 7, the mice were sacrificed and tissues were extracted and radioactivity counted using gamma counter to evaluate cell trafficking. PET images were normalized to units of SUV and presented as coronal sectional images.

### Statistical analysis

The data were compared using unpaired Student's *t*-test analyses. Differences were regarded as statistically significant for $p < 0.05$.

## Results

### Synthesis of $^{89}$Zr-DBN and cell labeling studies

$^{89}$Zr hydrogen phosphate was readily chelated by DFO-NCS to form $^{89}$Zr-DBN, with radiolabeling efficiency of 55% ± 5% after 1 h of reaction. This reaction mixture was then used directly for labeling of cells. The cell labeling efficiency using $^{89}$Zr-DBN was approximately 30% to 50% as determined by cell-bound radioactivity. Radioactivity concentrations of 0.50 ± 0.10, 0.47 ± 0.10, and 0.39 ± 0.20 MBq/$10^6$ cells were achieved when $6 \times 10^6$ cells were incubated for 30 min with approximately 6 MBq $^{89}$Zr-DBN with mMCs, hMSCs, and mDCs, respectively. In contrast, no cell labeling was observed using $^{89}Zr(HPO_4)_2$.

### Cellular proliferation and viability studies

The CyQUANT proliferation assay showed no difference in proliferation rate between unlabeled and $^{89}$Zr-labeled cells (Figure 2). Trypan blue cell viability tests were performed on radiolabeled cells immediately after labeling and up to 7 days post-labeling and compared with unlabeled cells. No change was observed in number of dead cells (blue-stained cells) over live cells (unstained cells) in both $^{89}$Zr-labeled and unlabeled cells, with percentage of dead cells <5% in all days tested.

### ApoTox-Glo viability/cytotoxicity and apoptosis assay

The ApoTox-Glo assay showed no loss in cellular viability and no increase in cytotoxicity or apoptosis in radiolabeled cells as illustrated in Figure 3. Viability was lost, and cytotoxicity enhanced when 30 μg/mL digitonin was added to cells (positive control), and apoptosis was increased with the addition of 2 μM staurosporine (positive control).

### Subcellular distribution of $^{89}$Zr radioactivity

At days 1, 4, and 7 after $^{89}$Zr labeling of mMCs, hMSCs, and mDCs, subcellular protein fractionation of the cells was performed. $^{89}$Zr radioactvity was incorporated predominantly (>99%) in hydrophobic membrane protein fraction of all cell types studied, strongly supporting the proposed mechanism of reaction of $^{89}$Zr-DBN with cell surface membrane protein to form a stable covalent bond.

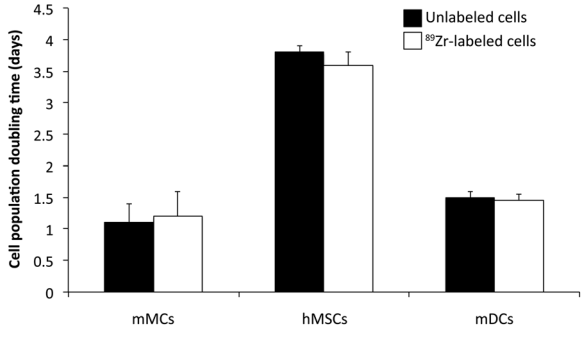


**Figure 2 Comparison of cell population doubling times for $^{89}$Zr-labeled and unlabeled mMCs, hMSCs and mDCs.** The cells were plated at appropriate cell number at day 3, and CyQUANT assay was performed at day 7 post-labeling. No significant differences were observed between radiolabeled and unlabeled cells. Values are shown as mean ± standard deviation, $n = 3$.

### Efflux of $^{89}$Zr radioactivity from labeled cells

Retention of $^{89}$Zr radioactivity by $^{89}$Zr-DBN-labeled cells was found to be stable in all the cells studied with negligible efflux observed over 7 days post-labeling (Figure 4).

### PET imaging and biodistribution studies in mice with intravenous injections

PET images and biodistribution data of intravenously administered $^{89}$Zr-labeled hMSCs and $^{89}Zr(HPO_4)_2$ in healthy mice are shown in Figure 5. The $^{89}$Zr-labeled hMSCs were concentrated primarily in the lung and liver, followed by the bone. On the other hand, $^{89}Zr(HPO_4)_2$ accumulated in the bone and liver and did not distribute to lung.

### *In vivo* tracking of stem cell engraftment in ischemia/reperfusion mouse model

Following myocardial delivery, $^{89}$Zr-labeled hMSCs (approximately 19.5% ± 9.5%) were retained for 7 days in the heart (Figure 6). The remaining cells were concentrated in the lung, followed by the bones and liver. The higher uptake in the lung relative to the liver is consistent with the biodistribution of $^{89}$Zr-labeled hMSCs released into the circulation (Figure 5).

## Discussion

Various strategies have been employed in the past to label cells with imaging isotopes for non-invasive *in vivo* cell tracking for cell-based therapies and infection imaging. Among them, $^{18}$F-FDG (for PET) [12-16] and $^{111}$In-oxine (for SPECT) [2-6], are the most widely used. Although $^{18}$F-FDG is useful for assessment of immediate delivery of cells and early fate of cells (approximately first few hours), it is not suited for *in vivo* cell tracking after 24 h post-injection due to its short half-life and poor retention in cells. Inability of $^{18}$F-FDG to allow cell tracking after 24 h limits its utility in cell-based therapies. For cell-based therapies, early engraftment period of 2 to 5 weeks post cell delivery is the most critical time period [20]. Therefore, imaging-based methods should be robust over this time frame to allow evaluation of various interventions for improving cell engraftment. The ability to monitor cells *in vivo* beyond 24 h is also of high importance for evaluation of infection using radiolabeled leukocytes. Conventional infection imaging protocols perform imaging at 1, 4, and 24 h post-injection to differentiate between inflammatory, acute infection, and chronic infection loci; however, in some patients, 48 h was necessary for reliable detection of infected lesions [21].

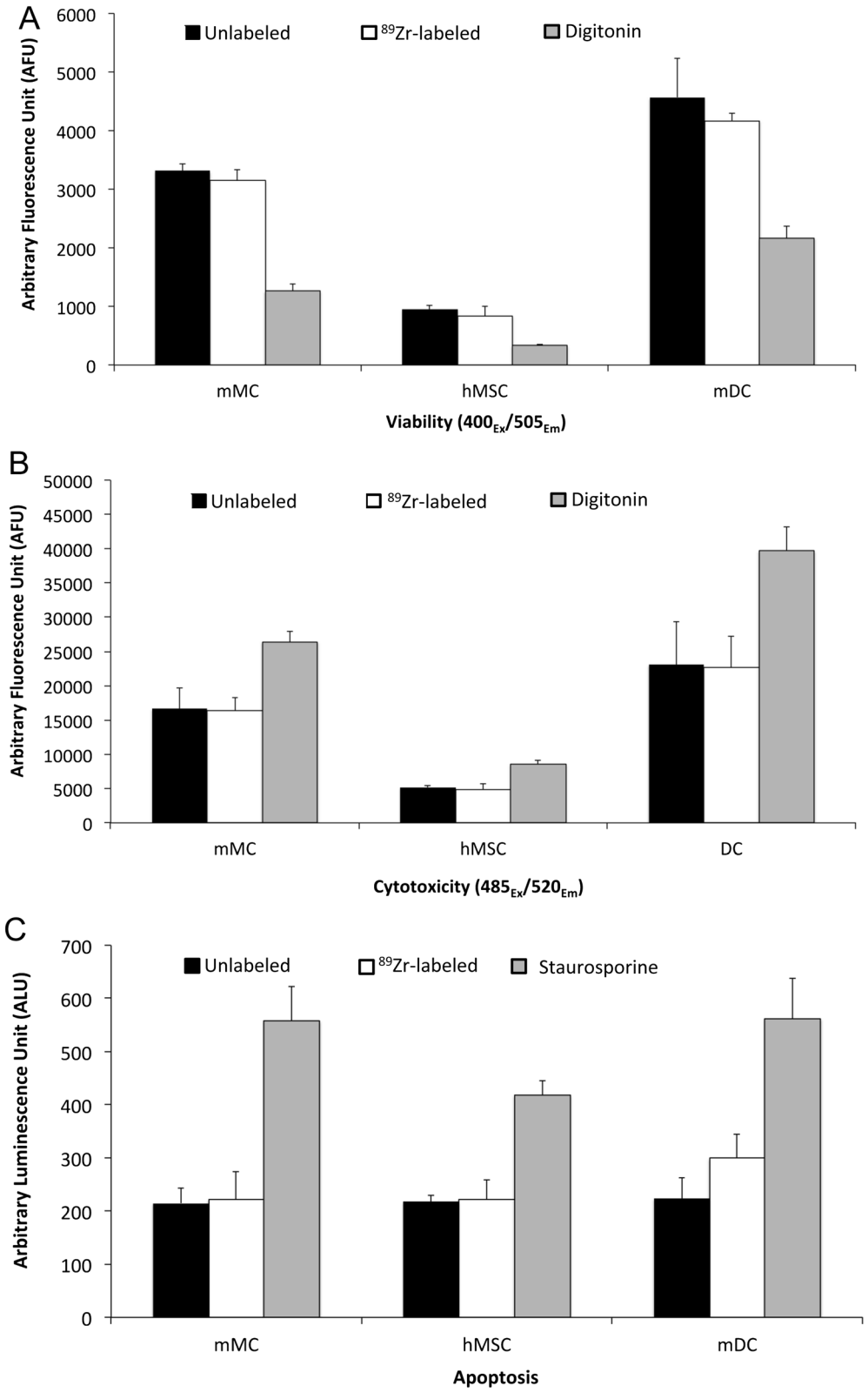


**Figure 3** (See legend on next page.)

(See figure on previous page.)
**Figure 3 Assessment of (A) viability, (B) cytotoxicity, and (C) apoptosis in $^{89}$Zr-labeled and unlabeled cells.** No statistically significant differences were observed between $^{89}$Zr-labeled and unlabeled cells after 7 days of culture with regard to viability, cytotoxicity, or apoptosis. As positive controls, 30 μg/mL digitonin was used for assays **(A)** and **(B)**, and 2 μM staurosporine for **(C)**. *$p < 0.05$ versus assessments in $^{89}$Zr-labeled and unlabeled cells using unpaired *t*-test. Values are shown as mean ± standard deviation, $n = 3$.

The use of $^{111}$In ($T_{1/2} = 2.8$ days) as a radiolabel for cell labeling allows longer observation periods for cell tracking but with lower spatial resolution of SPECT imaging. Cell labeling with $^{111}$In typically requires a lipophilic carrier molecule (e.g., oxine) for transporting the radiometal into cells [2-6]. After entering the cells, the radiometal then dissociates and gets trapped in the cell by binding to non-specific intracellular metal-binding proteins. The two major disadvantages of this approach are chemotoxicity of the lipophilic carrier molecule [22] and efflux of radiolabel from cells [2-6].

Recently, two groups (Charoenphun et al. [9] and Davidson-Moncada et al. [10]) reported synthesis of $^{89}$Zr-oxinate or $^{89}$Zr-oxine as a cell labeling reagent for PET-based cell tracking. As expected, both groups faced the problem of chemotoxicity and significant efflux of radioactivity from the cells post-labeling commonly associated with oxine-based labeling. Charoenphun et al. [9] showed reduced viability of $^{89}$Zr-oxine-labeled 5 T33 myeloma cells (from 93% to 76.3% ± 3.2% in the first 24 h) and significant efflux of radioactivity post-labeling (29% effluxed in 24 h). Davidson-Moncada et al. [10] also reported similar results with $^{89}$Zr-oxine-labeled human and rhesus macaques' natural killer cells. They observed a broad range of viability of 60% to 100% in the radiolabeled cells over the first 24 h, which declined to 20% to 30% after 6 days. A significant efflux of radioactivity was also observed in these viable $^{89}$Zr-oxine-labeled cells, approximately 20% to 25% effluxed in the first 24 h and 70% to 80% of radioactivity was effluxed after 7 days of culture. These drawbacks associated with the $^{89}$Zr-oxine labeling method compromises its utility for PET-based monitoring of *in vivo* cell trafficking.

To improve the stability of the $^{89}$Zr radiolabel on cells, we proposed $^{89}$Zr-DFO-NCS ($^{89}$Zr-DBN) as a labeling entity capable of forming covalent bonds with primary amines of cell surface protein (Figure 1). Since all cells express cell surface protein with exposed lysine residues and other primary amines, this strategy also provides a general labeling method to label a broad array of cells. The new strategy exploits both the strength of chelation of $^{89}$Zr by DFO with three hydroxamate groups (qualitative Zr-binding constant = approximately $10^{31}$) [23-26] as well as the inherent biostability of the thiourea bond that conjugates NCS group in $^{89}$Zr-DBN to primary amines of protein [27,28]. Furthermore, the labeling agent, $^{89}$Zr-DBN, is also expected to be well-tolerated by cells as opposed to toxic lipophilic carrier molecules like oxine, relying on the fact that DFO-NCS has been routinely used to conjugate DFO to IgG and IgM antibodies with no loss of antibody protein function [23,26-29]. The generality of the labeling target, along with the multiplicity of primary amines available on the cell surface, also avoids the specific targeting of highly sensitive processes that might affect cellular function or viability. In contrast to the previously noted $^{89}$Zr-oxine results [9,10], no efflux of radiolabel was observed from cultured cells labeled with $^{89}$Zr-DBN after repeated washing and culture with medium with 10% fetal bovine serum (FBS) out to 7 days. These data strongly argue for a covalent bonding of the radiolabel to the cells. Furthermore, in a subcellular fractionation study, essentially all $^{89}$Zr radioactivity was incorporated into the membrane bound

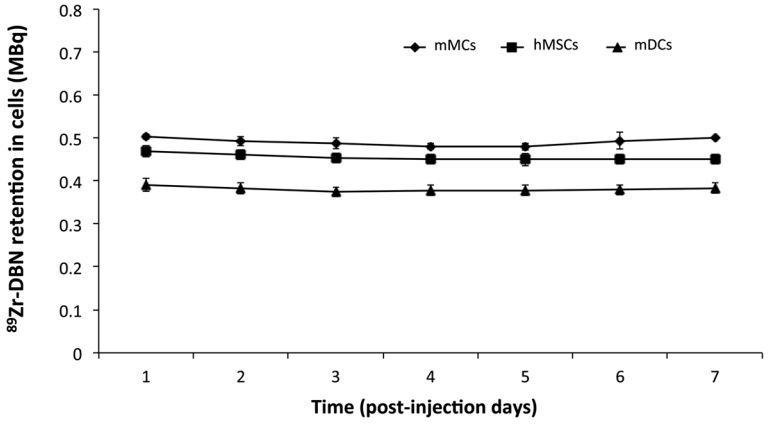


**Figure 4 Retention of $^{89}$Zr in $^{89}$Zr-labeled cells expressed as radioactivity in MBq in the cell population.** The retention value is representing total radioactivity/$10^6$ cells in the proliferating cell population. No significant change was observed in retention of $^{89}$Zr in radiolabeled cells. Values are shown as mean ± standard deviation, $n = 3$.

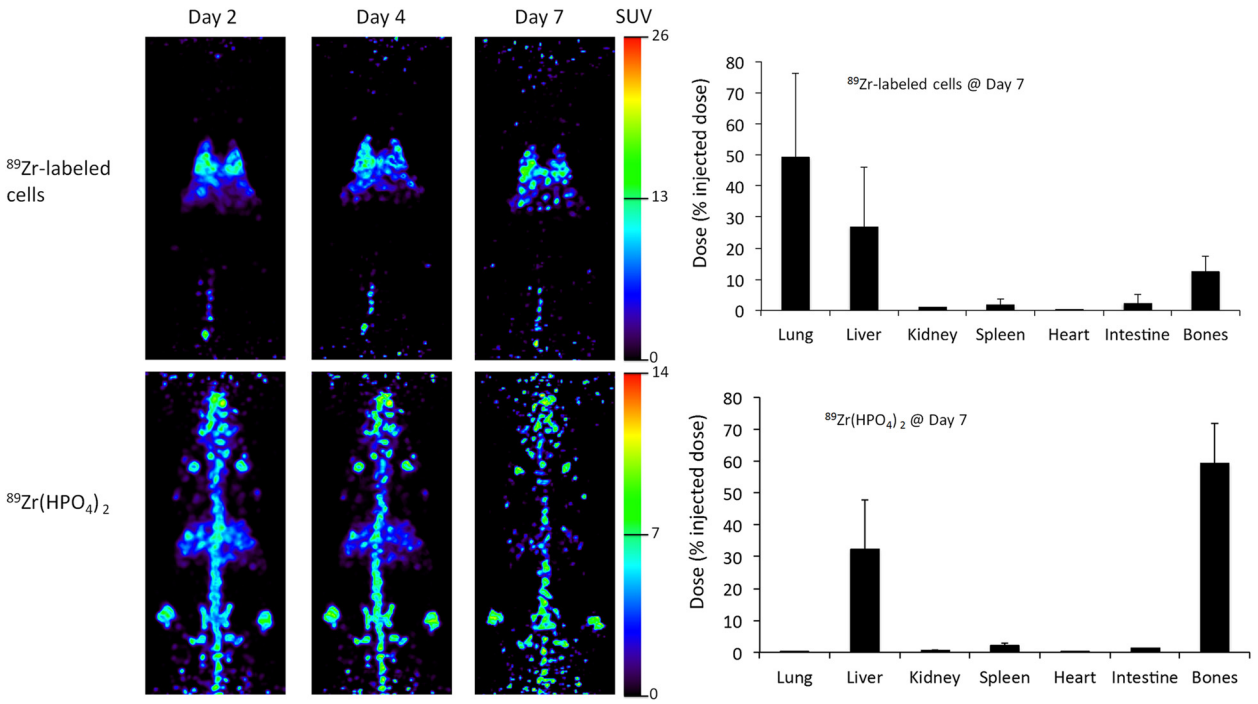


**Figure 5 Representative PET images and biodistribution data of $^{89}$Zr-labeled hMSCs and $^{89}$Zr$(HPO_4)_2$ following intravenous injection.** $^{89}$Zr-labeled human MSCs ($2 \times 10^5$ cells with radioactivity concentration approximately 0.37 MBq/$10^6$ cells) and $^{89}$Zr$(HPO_4)_2$ (approximately 0.074 MBq radioactivity) were intravenously injected in athymic mice. Most of the radioactivity was distributed in the lung, liver, and bones following injection of $^{89}$Zr-labeled hMSCs whereas most of the radioactivity was distributed in the liver and bones following injection of $^{89}$Zr$(HPO_4)_2$. Values in graphs are shown as mean ± standard deviation, $n = 3$.

protein fraction of the cells confirming the anticipated targeting of membrane protein. The targeting of cell-surface membrane protein also has the potential benefit of distancing the labeling agent from potentially sensitive sites in the cell. We found no evidence of chemotoxicity or radiotoxicity effects of $^{89}$Zr-DBN labeling of three cell types in the present study.

In this study, 30% to 50% labeling efficiencies were achieved with $^{89}$Zr-DBN in several cell types. The cell labeling yield for mMCs, hMSCs, and mDCs were 0.50 ± 0.10, 0.47 ± 0.10, and 0.39 ± 0.20 MBq/$10^6$ cells for mMCs, hMSCs, and mDCs, respectively. This is the maximum load of radioactivity per $10^6$ cells that we could achieve in this study. In the clinical setting, approximately $10^8$ cells

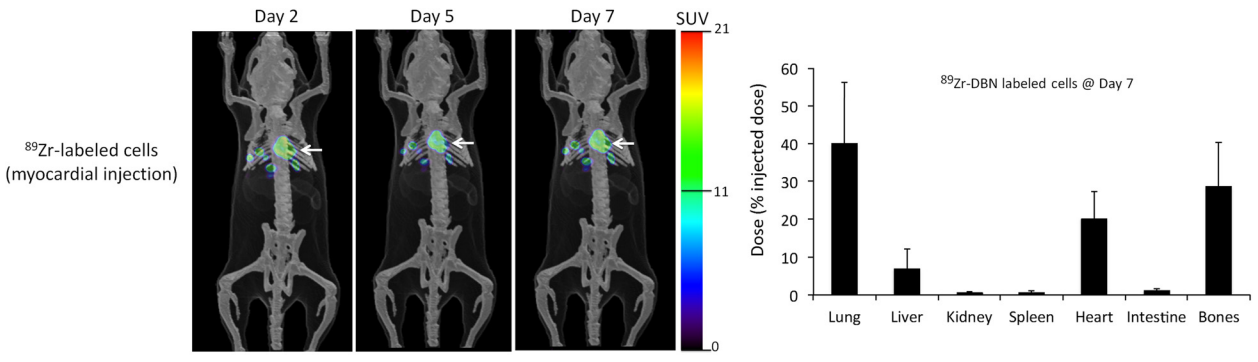


**Figure 6 Representative PET images and biodistribution data of $^{89}$Zr-labeled hMSCs following myocardial delivery.** $^{89}$Zr-labeled hMSCs ($2 \times 10^5$ cells with radioactivity concentration approximately 0.37 MBq/$10^6$ cells) were delivered to myocardium of an ischemia/reperfusion mouse model. Most of the radioactivity was distributed in the heart (arrow), lung, liver, and bones following myocardial delivery of $^{89}$Zr-labeled hMSCs. Values in graph are shown as mean ± standard deviation, $n = 5$.

are typically delivered to patients. Based on the labeling yield obtained in this study, the amount of $^{89}$Zr radioactivity administered to a patient would be in the range 30 to 50 MBq (0.8 to 1.4 mCi), which is in the range of $^{89}$Zr radioactivity that is currently being used in patients with $^{89}$Zr-labeled antibodies.

After encouraging *in vitro* validation tests, we performed *in vivo* validations by investigating the biodistribution of $^{89}$Zr-labeled hMSCs after intravenous injection in athymic nude mice for 7 days post-injection. Trapping of MSCs in the lungs following intravenous injection is well documented [30,31]. Therefore, we expected major accumulation of $^{89}$Zr-labeled human MSCs in mouse lungs following intravenous injection with slow clearance. With time, cells were expected to dislodge from this physical pulmonary entrapment and distribute to other organs. As expected, the majority of intravenously injected $^{89}$Zr-labeled hMSCs were trapped in the lung (50% ± 27%) and the remainder was found in the liver (27% ± 19%) and bones (16% ± 5%) after 7 days post-injection, which are expected homing sites for injected mesenchymal stem cells after dislodging from the lung [32,33]. This was in contrast to the biodistribution of $^{89}Zr(HPO_4)_2$, which distributed primarily in the bone (59% ± 13%) and liver (32% ± 15%) but did not accumulate in lungs. The distinct biodistributions of $^{89}$Zr-labeled hMSCs and $^{89}Zr(HPO_4)_2$, together with the stability of radiolabel and lack of cytotoxicity, strongly support the robustness of the $^{89}$Zr-DBN-based cell labeling approach.

To further test the application of $^{89}$Zr-labeled hMSCs, we performed a stem cell engraftment study using a myocardial acute ischemia/reperfusion mouse model. $^{89}$Zr-labeled hMSCs were delivered to the myocardium of athymic mice following an acute myocardial ischemia/reperfusion insult. After 7 days post-delivery, $^{89}$Zr-labeled hMSCs were found in the heart (20% ± 7%), lung (40% ± 16%), bone (29% ± 11%), and liver (7% ± 5%). The observed retention in the heart is in accordance with previously published work on hMSC engraftment estimated by invasive quantitative PCR method in a similar rodent model [34].

Low levels of *in vitro* demetalation of $^{89}$Zr-DFO complexes (2% to 3%/week) in serum at 37°C have been reported [23,29], and clinical studies using $^{89}$Zr-DFO-labeled antibodies out to 7 days have yet to show significant bone uptake of $^{89}$Zr indicative of demetalation [35-39]. Our initial findings of distribution of $^{89}$Zr-labeled hMSCs in mouse models confirm the biostability of the radiolabel bound to the DFO moiety supporting further exploration of the $^{89}$Zr-DBN labeling method for monitoring stem cell engraftment and cell trafficking. Extension of this approach with the use of an alternative zirconium chelator, such as 3,4,3-[LI-1,2-HOPO] [40] may further improve the biostability of the labeling agent.

## Conclusions

The $^{89}$Zr-DBN labeling agent is shown to be a robust, general, and biostable cell labeling strategy for PET-based non-invasive *in vivo* cell tracking. To explore the full potential of this approach, more work is needed to test this strategy in various model systems and disease processes that are germane to cell trafficking and stem cell therapies. We have ongoing efforts to define the imaging sensitivity, biostability, and toxicity parameters as the limits are pushed toward higher $^{89}$Zr radioactivity loading of cells and longer observation periods *in vivo.*

### Compliance with ethical standards

1. Disclosure of potential conflicts of interest: no authors have affiliations that present financial or non-financial competing interests for this work.
2. Research involving human participants and/or animals:
   - All procedures performed in studies involving human participants were in accordance with the ethical standards of the institutional and/or national research committee and with the 1964 Helsinki declaration and its later amendments or comparable ethical standards. The patient-derived mesenchymal stem cells were obtained in compliance with institutional ethical review board guidance.
   - All applicable international, national, and/or institutional guidelines for the care and use of animals were followed. All procedures performed in studies involving animals were under approval and in accordance with the Ethical Standards of Mayo Clinic Institutional Animal Care and Use Committee.
3. Informed consent: informed consent was obtained from all individual participants included in the study.

#### Abbreviations

$^{89}Zr(HPO_4)_2$: zirconium hydrogen phosphate; Alpha MEM: alpha modified Eagle's medium; Anti-CD45: antibody against cluster of differentiation-45 antigen; DBN: desferrioxamine-NCS; DFO-Bz-NCS: desferrioxamine-benzyl-sodium thiocyanate; DMEM: Dulbecco's modified Eagle's medium; DTPA: diethylene triamine pentaacetic acid; FBS: fetal bovine serum; FDG: $^{18}$F-2-fluoro-2-deoxy-D-glucose; GM-CSF: granulocyte-macrophage colony-stimulating factor; HBSS: Hank's Balanced Salt Solution; HEPES-KOH: (4-(2-hydroxyethyl)-1-piperazineethanesulfonic acid)-potassium hydroxide; HMPAO: hexamethylpropyleneamine oxime; hMSCs: human mesenchymal stem cells; IgG: immunoglobulin G; IgM: immunoglobulin M; iTLC: instant thin layer chromatography; $K_2CO_3$: potassium carbonate; $K_2HPO_4/KH_2PO_4$: dipotassium hydrogen phosphate/potassium hydrogen phosphate; MBq: megabecquerel; mDCs: mouse-derived dendritic cells; MIPs: maximal images projection; mMCs: mouse-derived melanoma cells; PET: positron emission tomography; PTSM: pyruvaldehyde-bis (N4-methylthiosemicarbazone); Rf: retention factor; SPECT: single-photon emission computerized tomography; $T_{1/2}$: half-life of radioisotope.

#### Competing interests

The authors declare that they have no competing interests.

**Authors' contributions**

AB participated in the standardization of cell labeling conditions and development of the cell labeling agent, in performing *in vitro/in vivo* validation studies along with image/data analysis and statistical analysis and drafting the manuscript. MKP participated in the development of the synthesis process for $^{89}$Zr from solution target, in development of the process of elution of $^{89}$Zr in the form of zirconium hydrogen phosphate and in development of the cell labeling agent. YED participated in the elution of $^{89}$Zr in the form of zirconium hydrogen phosphate and analysis of cell labeling and retention data. JJN performed the surgery for developing the ischemia/reperfusion mouse model and performed intra-myocardial stem cell injections. RJC participated in the procurement and establishment of human-derived stem cell lines. AT contributed the ischemia/reperfusion mouse model with procured human stem cells for testing the stability of the label in labeled cells *in vivo*. ABehfar conceived the idea and coordinated the execution of ischemia/reperfusion mouse model with human stem cells for testing the stability of the label in labeled cells in *in vivo* environment. TRD conceived the $^{89}$Zr-DBN labeling agent, participated in the experimental design, coordination of the research team, and helped to draft the manuscript. All authors read and approved the final manuscript.

**Acknowledgements**

The work was funded by the Mayo Clinic Department of Radiology and Mayo Clinic Center for Regenerative Medicine.

**Author details**

[1]Department of Radiology, Mayo Clinic, Rochester 55905, MN, USA. [2]Division of Cardiovascular Diseases, Mayo Clinic, Rochester 55905, MN, USA.

Received: 27 January 2015 Accepted: 13 March 2015
Published online: 28 March 2015

**References**

1. Nguyen PK, Riegler J, Wu JC. Stem cell imaging: from bench to bedside. Cell Stem Cell. 2014;14:431–44.
2. Gildehaus FJ, Haasters F, Drosse I, Wagner E, Zach C, Mutschler W, et al. Impact of indium-111 oxine labelling on viability of human mesenchymal stem cells in vitro, and 3D cell-tracking using SPECT/CT in vivo. Mol Imaging Biol. 2011;13:1204–14.
3. Hughes DK. Nuclear medicine and infection detection: the relative effectiveness of imaging with $^{111}$In-oxine-, $^{99m}$Tc-HMPAO-, and $^{99m}$Tc-stannous fluoride colloid-labeled leukocytes and with $^{67}$Ga-citrate. J Nucl Med Tech. 2003;31:196–201.
4. Kuyama J, McCormack A, George AJ, Heelan BT, Osman S, Batchelor JR, et al. Indium-111 labelled lymphocytes: isotope distribution and cell division. Eur J Nucl Med. 1997;24:488–96.
5. Brenner W, Aicher A, Eckey T, Massoudi S, Zuhayra M, Koehl U, et al. 111In-labeled CD34+ hematopoietic progenitor cells in a rat myocardial infarction model. J Nucl Med. 2004;45:512–8.
6. Roca M, de Vries EF, Jamar F, Israel O, Signore A. Guidelines for the labelling of leucocytes with $^{(111)}$In-oxine. Inflammation/Infection Taskgroup of the European Association of Nuclear Medicine. Eur J Nucl Med Mol Imaging. 2010;37:835–41.
7. Adonai N, Nguyen KN, Walsh J, Iyer M, Toyokuni T, Phelps ME, et al. Ex vivo cell labeling with $^{64}$Cu-pyruvaldehyde-bis(N4-methylthiosemicarbazone) for imaging cell trafficking in mice with positron-emission tomography. Proc Nat Acad Sci. 2002;99:3030–5.
8. Tarantal AF, Lee CC, Kukis DL, Cherry SR. Radiolabeling human peripheral blood stem cells for positron emission tomography (PET) imaging in young rhesus monkeys. PLoS One. 2013;8:e77148.
9. Charoenphun P, Meszaros LK, Chuamsaamarkkee K, Sharif-Paghaleh E, Ballinger JR, Ferris TJ, et al. [$^{89}$Zr]Oxinate for long-term in vivo cell tracking by positron emission tomography. Eur J Nucl Med Mol Imaging. 2015;42:278–87.
10. Davidson-Moncada J, Sato N, Hoyt Jr, Reger RN, Thomas M, Clevenger R, et al. A novel method to study the in vivo trafficking and homing of adoptively transferred NK cells in rhesus macaques and humans. Proceedings of the 56th Annual Meeting of the American Society of Hematology, San Francisco, CA, December 6–9, 2014. Abstract #659.
11. Sato N, S.L., Choyke P, Cell labeling using Zr-89 - comparison with In-111 oxine. Proceedings World Molecular Imaging Congress, Savannah, GA, 2013, 2013: p. P533.
12. Stojanov K, de Vries EF, Hoekstra D, van Waarde A, Dierckx RA, Zuhorn IS. [$^{18}$F]FDG labeling of neural stem cells for in vivo cell tracking with positron emission tomography: inhibition of tracer release by phloretin. Mol Imaging. 2012;11:1–12.
13. Zhang Y, Dasilva JN, Hadizad T, Thorn S, Kuraitis D, Renaud JM, et al. $^{18}$F-FDG cell labeling may underestimate transplanted cell homing: more accurate, efficient, and stable cell labeling with hexadecyl-4-[$^{18}$F] fluorobenzoate for in vivo tracking of transplanted human progenitor cells by positron emission tomography. Cell Transplant. 2012;21:1821–35.
14. Meier R, Piert M, Piontek G, Rudelius M, Oostendorp RA, Senekowitsch-Schmidtke R, et al. Tracking of [$^{18}$F]FDG-labeled natural killer cells to HER2/neu-positive tumors. Nucl Med Biol. 2008;35:579–88.
15. Doyle B, Kemp BJ, Chareonthaitawee P, Reed C, Schmeckpeper J, Sorajja P, et al. Dynamic tracking during intracoronary injection of $^{18}$F-FDG-labeled progenitor cell therapy for acute myocardial infarction. J Nucl Med. 2007;48:1708–14.
16. Pellegrino D, Bonab AA, Dragotakes SC, Pitman JT, Mariani G, Carter EA. Inflammation and infection: imaging properties of $^{18}$F-FDG-labeled white blood cells versus $^{18}$F-FDG. J Nucl Med. 2005;46:1522–30.
17. de Vries EF, Roca M, Jamar F, Israel O, Signore A. Guidelines for the labelling of leucocytes with $^{99m}$Tc-HMPAO. Inflammation/Infection Taskgroup of the European Association of Nuclear Medicine. Eur J Nucl Med Mol Imaging. 2010;37:842–8.
18. Pandey MK, Engelbrecht HP, Byrne JP, Packard AB, DeGrado TR. Production of $^{89}$Zr via the $^{89}$Y(p, n)$^{89}$Zr reaction in aqueous solution: effect of solution composition on in-target chemistry. Nucl Med Biol. 2014;41:309–16.
19. Holland JP, Sheh Y, Lewis JS. Standardized methods for the production of high specific-activity zirconium-89. Nucl Med Biol. 2009;36:729–39.
20. Naumova AV, Modo M, Moore A, Murry CE, Frank JA. Clinical imaging in regenerative medicine. Nat Biotech. 2014;32:804–18.
21. Glaudemans AW, Galli F, Pacilio M, Signore A. Leukocyte and bacteria imaging in prosthetic joint infection. Eur Cell Mater. 2013;25:61–77.
22. Kassis AI, Adelstein SJ. Chemotoxicity of indium-111 oxine in mammalian cells. J Nucl Med. 1985;26:187–90.
23. Holland JP, Divilov V, Bander NH, Smith-Jones PM, Larson SM, Lewis JS. $^{89}$Zr-DFO-J591 for immunoPET of prostate-specific membrane antigen expression in vivo. J Nucl Med. 2010;51:1293–300.
24. Keberle H. The biochemistry of desferrioxamine and its relation to iron metabolism. Annals N Y Acad Sci. 1964;119:758–68.
25. Takagai Y, Takahashi A, Yamaguchi H, Kubota T, Igarashi S. Adsorption behaviors of high-valence metal ions on desferrioxamine B immobilization nylon 6,6 chelate fiber under highly acidic conditions. J Colloid Interface Sci. 2007;313:359–62.
26. Deri MA, Zeglis BM, Francesconi LC, Lewis JS. PET imaging with $^{89}$Zr: from radiochemistry to the clinic. Nucl Med Biol. 2013;40:3–14.
27. Vosjan MJ, Perk LR, Visser GW, Budde M, Jurek P, Kiefer GE, et al. Conjugation and radiolabeling of monoclonal antibodies with zirconium-89 for PET imaging using the bifunctional chelate p-isothiocyanatobenzyl-desferrioxamine. Nat Protoc. 2010;5:739–43.
28. Perk LR, Vosjan MJ, Visser GW, Budde M, Jurek P, Kiefer GE, et al. p-Isothiocyanatobenzyl-desferrioxamine: a new bifunctional chelate for facile radiolabeling of monoclonal antibodies with zirconium-89 for immuno-PET imaging. Eur J Nucl Med Mol Imaging. 2010;37:250–9.
29. Dijkers ECF, Kosterink JGW, Rademaker AP, Perk LR, van Dongen GAMS, Bart J, et al. Development and characterization of clinical-grade Zr-89-trastuzumab for HER2/neu immunoPET imaging. J Nucl Med. 2009;50:974–81.
30. Schrepfer S, Deuse T, Reichenspurner H, Fischbein MP, Robbins RC, Pelletier MP. Stem cell transplantation: the lung barrier. Transplant Proc. 2007;39:573–6.
31. Fischer UM, Harting MT, Jimenez F, Monzon-Posadas WO, Xue H, Savitz SI, et al. Pulmonary passage is a major obstacle for intravenous stem cell delivery: the pulmonary first-pass effect. Stem Cells Dev. 2009;18:683–92.
32. Gao J, Dennis JE, Muzic RF, Lundberg M, Caplan AI. The dynamic in vivo distribution of bone marrow-derived mesenchymal stem cells after infusion. Cells Tissues Organs. 2001;169:12–20.
33. Daldrup-Link HE, Rudelius M, Metz S, Piontek G, Pichler B, Settles M, et al. Cell tracking with gadophrin-2: a bifunctional contrast agent for MR

imaging, optical imaging, and fluorescence microscopy. Eur J Nucl Med Mol Imaging. 2004;31:1312–21.
34. Terrovitis J, Lautamaki R, Bonios M, Fox J, Engles JM, Yu J, et al. Noninvasive quantification and optimization of acute cell retention by in vivo positron emission tomography after intramyocardial cardiac-derived stem cell delivery. J Am Coll Cardiol. 2009;54:1619–26.
35. Boerjesson PKE, Jauw YWS, de Bree R, Roos JC, Castelijns JA, Leemans CR, et al. Radiation dosimetry of Zr-89-labeled chimeric monoclonal antibody U36 as used for immuno-PET in head and neck cancer patients. J Nucl Med. 2009;50:1828–36.
36. Borjesson PKE, Jauw YWS, Boellaard R, de Bree R, Comans EFI, Roos JC, et al. Performance of immuno-positron emission tomography with zirconium-89-labeled chimeric monoclonal antibody U36 in the detection of lymph node metastases in head and neck cancer patients. Clin Cancer Res. 2006;12:2133–40.
37. Rizvi SNF, Visser OJ, Vosjan MJWD, van Lingen A, Hoekstra OS, Zijlstra JM, et al. Biodistribution, radiation dosimetry and scouting of Y-90-ibritumomab tiuxetan therapy in patients with relapsed B-cell non-Hodgkin's lymphoma using Zr-89-ibritumomab tiuxetan and PET. Eur J Nucl Med Mol Imaging. 2012;39:512–20.
38. Dijkers EC, Munnink THO, Kosterink JG, Brouwers AH, Jager PL, de Jong JR, et al. Biodistribution of Zr-89-trastuzumab and PET imaging of HER2-positive lesions in patients with metastatic breast cancer. Clin Pharmacol Ther. 2010;87:586–92.
39. Gaykema SB, Brouwers AH, Lub-de Hooge MN, Pleijhuis RG, Timmer-Bosscha H, Pot L, et al. $^{89}$Zr-bevacizumab PET imaging in primary breast cancer. J Nucl Med. 2013;54:1014–8.
40. Deri MA, Ponnala S, Zeglis BM, Pohl G, Dannenberg JJ, Lewis JS, et al. Alternative chelator for $^{89}$Zr radiopharmaceuticals: radiolabeling and evaluation of 3,4,3-(LI-1,2-HOPO). J Med Chem. 2014;57:4849–60.